Comparing the RTM and PSPI migrations to estimate the gradient using the fast waveform inversion

Marcelo Guarido*, Sergio J. Romahn*, Laurence R. Lines*, Robert J. Ferguson†, Kristopher A. H. Innanen*

ABSTRACT

The gradient that optimize the model update in the full waveform routine is mainly obtained by a reverse-time migration of the residuals. However, if we can interpret the whole routine as a combination of seismic processing tools, we believe it is possible to obtain the gradient using any kind of depth migration. In this paper, we are comparing the use of RTM and PSPI migration to estimate the gradient, using the post-stack forward modeling-free approximations of the FWI, the FastWI. The inverted models using RTM and PSPI migrations have similar resolution in a simple velocity model, with the advantage of the PSPI been cheaper, but the RTM may lead to more continuous and high resolution models on more complex geologies.

INTRODUCTION

Seismic inversion techniques are the ones that use intrinsic informations contained in the data to determine rock properties by matching a model that "explains" the data. Some examples are the variation of amplitude per offset, or AVO (Shuey, 1985; Fatti et al., 1994), the traveltime differences between traces, named traveltime tomography (Langan et al., 1984; Bishop and Spongberg, 1984; Cutler et al., 1984), or even by matching synthetic data to the observed data, as it is done in full waveform inversion (Tarantola, 1984; Virieux and Operto, 2009; Margrave et al., 2010; Pratt et al., 1998), among others. These inversions can compute rock parameters as P and S waves velocities, density, viscosity and others. In this work I am focused in the inversion of the P wave velocity.

FWI is a least-square based inversion, which objective is to find the model parameters that minimizes the difference between observed (acquired) and synthetic shots (Margrave et al., 2011), or the residuals. This is accomplished in an iterative fit method by linearizing a non-linear problem. It is an algorithm similar to a *Ridge Regression* (Chipman, 1999), which minimizes non-linear problems by adding a regularization term to avoid over fitting (to smooth the model). In seismic processing, I regularize the inversion by convolving the model with a 2D Gaussian window (Margrave et al., 2010).

The full waveform inversion was proposed in the early 80's (Pratt et al., 1998) but the technique was considered too expensive in computational terms. Lailly (1983) and Tarantola (1984) simplified the methodology by using the steepest-descent method (or gradient method) in the time domain to minimize the objective function without calculate, explicitly, the partial derivatives. They compute the gradient by a reverse-time migration (RTM) of the residuals. Pratt et al. (1998) develop a matrix formulation for the full waveform inver-

*CREWES - University of Calgary
†University of Calgary

sion in the frequency domain and present more efficient ways to compute the gradient and the inverse of the Hessian matrix (the sensitive matrix) the Gauss-Newton or the Newton approximations. The FWI is shown to be more efficient if applied in a multi-scale method, where lower frequencies are inverted first and is increased as more iterations are done (Pratt et al., 1998; Virieux and Operto, 2009; Margrave et al., 2010). An overview of the FWI theory and studies are compiled by Virieux and Operto (2009). Lindseth (1979) showed that an impedance inversion from seismic data is not effective due to the lack of low frequencies during the acquisition but could be compensated by the match with a sonic-log profile. Warner and Guasch (2014) use the deviation of the Weiner filters of the real and estimated data as the object function with great results. Margrave et al. (2010) and Romahn and Innanen (2016) calibrate the gradient by matching it with sonic logs, estimating a more precise step length and avoiding cycle skipping. They also use the Gazdag and Sguazzero (1984) PSPI migration algorithm with a deconvolution imaging condition (Margrave et al., 2011; Wenyong et al., 2013) to migrate the residuals faster than the RTM, but preserving the gradient's resolution. Guarido et al. (2015) use the PSPI migration to migrate each frequency content of the residuals independently, generating a pseudo-gradient for each frequency and then averaging stacking them, using the step length as weight. It resulted on a highly detailed model, but the computation costs are high. Guarido et al. (2016) apply an impedance inversion in the gradient to improve the resolution of the inverted model. Guarido et al. (2016, 2017b) propose a simpler approximation for the gradient that does not require any forward modeling. They just apply a PSPI migration on the acquired data and compare the result with the current model. The methodology was also extended for a post-stack depth migration. However, two forward modeling are required to estimate the step length. Guarido et al. (2017a) combines the forward modeling-free gradient with the well calibration (Margrave et al., 2010; Romahn and Innanen, 2016) to create a 100% forward modeling-free FWI, that can be applied using pre or post stack migrations. The post-stack approximation of the FWI is a linear approximation of the seismic processing steps to obtain the gradient, and is named *Fast Waveform Inversion*, or simply FastWI.

In this report, we are comparing the use of the RTM and PSPI migrations to obtain the gradient. The tests are done, initially, in a simple velocity model using the FastWI with well calibration from Guarido et al. (2017a). Later, the comparison is done on the Marmousi model, to understand the behavior of the updates on a complex geology.

THEORY

The steepest-descent method

The objective function of the FWI method is (Tarantola, 1984):

$$C(\mathbf{m}) = ||\mathbf{d}_0 - \mathbf{d}(\mathbf{m})||^2 = ||\Delta\mathbf{d}(\mathbf{m})||^2 \tag{1}$$

where Δd is the data residual (the difference between acquired and synthetic shots), m is the model (in this work, the P-wave velocity) and $||$ represents the norm-2 of the array. The minimization is done by calculating the Taylor's expansion of the objective function of the equation 1 around a perturbation δm of the model and taking the derivative equal to zero

(Tarantola, 1984; Pratt et al., 1998; Virieux and Operto, 2009). The solution is:

$$\mathbf{m}_{n+1} = \mathbf{m}_n - H_n^{-1}\mathbf{g}_n \tag{2}$$

where H is the Hessian (or sensitive matrix), g is the gradient computed by back-propagating the data residual and n is the *n-th* iteration. It is known as the Newton method. For the steepest-descent method, the Hessian matrix can be neglected and be equalized to the identity matrix:

$$\mathbf{m}_{n+1} = \mathbf{m}_n - \alpha_n\mathbf{g}_n \tag{3}$$

where α is the step length, which can be determinded by a line search or a least squares minization (Pica et al., 1990). At this part, the gradient is understood as the reverse-time migration ot the residuals. We can interpret this step and expand its meaning to say that the gradient is equivalent to a pre-stack depth migration of the residuals, and we decided to use a PSPI migration of the residuals with a deconvolution imaging condition (Margrave et al., 2010, 2011; Wenyong et al., 2013; Guarido et al., 2014).

The forward modeling-free gradient

Computing the gradient requires three very known seismic processing steps: PSDM of the residuals, stacking and impedance inversion. Let's understand those steps as the operators *M* for migration, *S* for stacking and *I* for impedance inversion. Equation 3 can be re-written as:

$$\begin{aligned}\mathbf{m}_{n+1} &= \mathbf{m}_n - \alpha_n\mathbf{g}_n \\ &= \mathbf{m}_n - \alpha_n I\left\{S\left[M\left(\Delta\mathbf{d}(\mathbf{m_n})\right)\right]\right\} \\ &= \mathbf{m}_n - \alpha_n I\left\{S\left[M\left(\mathbf{d}_0 - \mathbf{d}(\mathbf{m_n})\right)\right]\right\}\end{aligned} \tag{4}$$

where $\Delta\mathbf{d}(\mathbf{m_n})$ is the n-th iteration residual $\mathbf{d}_0 - \mathbf{d}(\mathbf{m_n})$, $\mathbf{d}_0$ is the acquired data, $\mathbf{d}(\mathbf{m_n})$ is the synthetic data of the n-th iteration and $\mathbf{m_n}$ is the n-th iteration inverted model. For simplification and easier visualization, let's set $\mathbf{d}(\mathbf{m_n}) = \mathbf{d_n}$. Then equation 4 is:

$$\mathbf{m}_{n+1} = \mathbf{m}_n - \alpha_n I\left\{S\left[M\left(\mathbf{d}_0 - \mathbf{d_n}\right)\right]\right\} \tag{5}$$

Considering the linearity property of the migration operator (see appendix), the acquired and synthetic shots can be migrated separately:

$$\mathbf{m}_{n+1} = \mathbf{m}_n - \alpha_n I\left\{S\left[M\left(\mathbf{d}_0\right) - M\left(\mathbf{d_n}\right)\right]\right\} \tag{6}$$

The next step is to use the linearity property of the stacking operator and equation 6 becomes:

$$\mathbf{m}_{n+1} = \mathbf{m}_n - \alpha_n I \left\{ S \left[M \left(\mathbf{d}_0 \right) \right] - S \left[M \left(\mathbf{d_n} \right) \right] \right\} \tag{7}$$

The impedance inversion operator is *approximately* linear if we assume that the Earth's impedance follow a linear trend (small reflection coefficients) and a Taylor expansion of the reflection coefficients is used to estimate the update as a perturbation of Earth's impedance, ending up with another solution for equation 7:

$$\mathbf{m}_{n+1} = \mathbf{m}_n - \alpha_n (I \left\{ S \left[M \left(\mathbf{d}_0 \right) \right] \right\} - \underbrace{I \left\{ S \left[M \left(\mathbf{d_n} \right) \right] \right\}}_{\text{Current model}}) \tag{8}$$

Again, on the second hand of the gradient approximation we have the model of the current iteration $\mathbf{m}_n$. Then equation 8 is simplified to:

$$\mathbf{m}_{n+1} = \mathbf{m}_n - \alpha_n (I \left\{ S \left[M \left(\mathbf{d}_0 \right) \right] \right\} - \mathbf{m}_n) \tag{9}$$

Equation 9 understand the gradient as a residual impedance inversion of the acquired data relative to the current model. The objective function is being minimized on the estimation of the step length, that requires 2 forward modeling when using Pica et al. (1990)'s approximation.

Looking again at equation 9, we understand that we are estimating the gradient by applying a sequence seismic processing tools. If we think about migration and stack, migrating the data and stacking should have the same effect as doing the inverted process (the pre and post stack migrations outputs have the same physical meaning: an image of the reflection coefficients of the subsurface). Then equation 9 is equivalent to:

$$\mathbf{m}_{n+1} = \mathbf{m}_n - \alpha_n (I \left\{ M \left[S \left(\mathbf{d}_0 \right) \right] \right\} - \mathbf{m}_n) \tag{10}$$

This means we can input in the algorithm a stacked section (figure 1 is the stacked section used in the first test using a simple model) and apply a post-stack depth migration algorithm (we used a zero-offset based PSPI with a cross-correlation imaging condition). The stacking velocity used to obtain the stacked section of figure 1 is the initial model of figure 3 converted to RMS velocity. The direct arrivals are removed (muted) to avoid artifacts in the shallow area, but it means that the inversion is not effective in the near surface (as some primaries ended up muted as well).

Analyzing the stacked section on figure 1, we noticed the presence of diffractions on the center area of the model caused by the fault zones. We can also observe a strong horizontal event close to the surface and also internal multiples are very evident on the deeper areas. We took note of all those observations and studied how they affected the inversion.

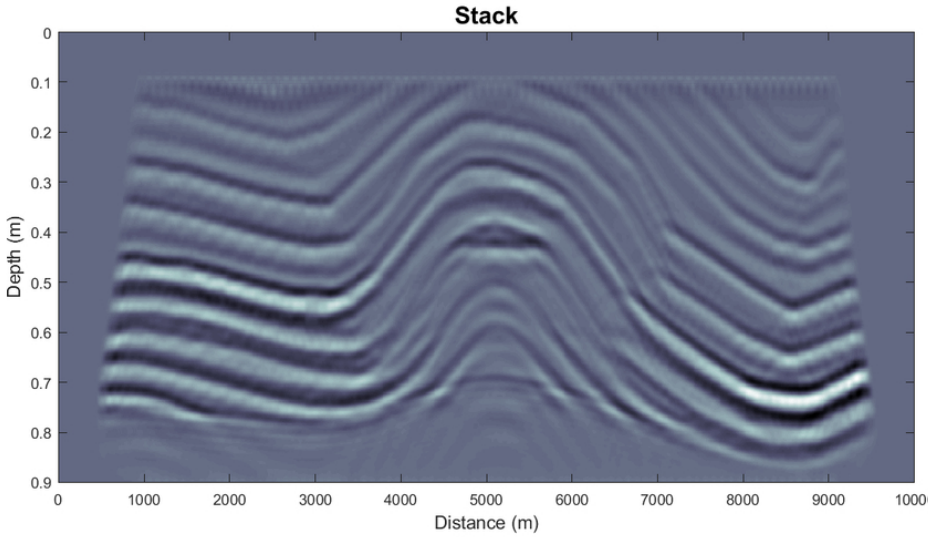

FIG. 1. Stacked section used as input in the post-stack method.

Well calibration

Until now we are assuming Pica et al. (1990)'s approximation to determine the step length on equations 9 and 10. However, it goes against our seeking for a forward modeling-free routine, as they still require two forward modeling to estimate the step length. Margrave et al. (2010) and Romahn and Innanen (2016) calibrate the gradient by matching it with a sonic log at the same spatial location. They estimate a scalar and phase rotation to create a match filter to convolve with the gradient. This would lead us with a FWI algorithm 100% forward modeling-free. So we decided to implement it.

To find the scalar α that minimizes the impedance inverted gradient trace S_{grad} to the impedance (sonic log) well trace S_{well}, we minimize the L2-norm function for α:

$$\Phi = ||S_{well} - \alpha S_{grad}||^2 \tag{11}$$

This leads to a simple equation to estimate α:

$$\alpha = \frac{S_{well}^T S_{grad}}{S_{grad}^T S_{grad}} \tag{12}$$

For the phase rotation, we use the $Toolbox$ code $constphase.m$ that finds the angle ϕ that makes S_{grad} looks like S_{well}. By finding α and ϕ, we create a matching filter which is convolved with the gradient to have the model update.

Combining the well tie calibration with the forward modeling-free gradient of equations 9 and 10, the FWI routine can be executed 100% forward modeling-free. This reduces significantly the cost of the inversion without the need of the source estimation. The post-stack inversion with well calibration is named ***FastWI***.

SIMULATION

FastWI RTM vs PSPI: Simple Model

Initially, we are testing the difference of the RTM and PSPI migrations in the forward-modeling post-stack approximation. Synthetic data were created using the model of figure 2, where the three black lines are the wells positions for the gradient calibration. A matching filter is obtained for each well and are interpolated, resulting in a matching filter for each trace. The input data is the stacked section of figure 1. In both test, a multi-scale method is used (inversion of low frequencies first and the high frequencies in sequence).

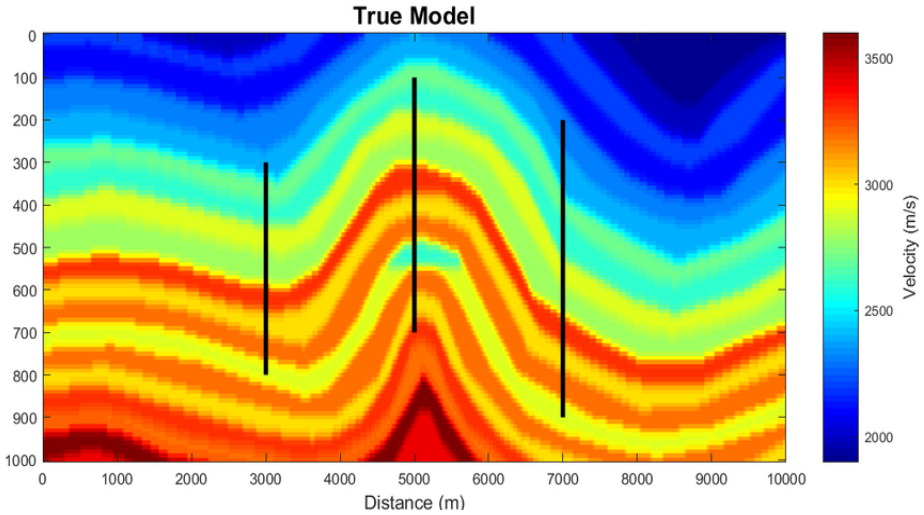

FIG. 2. True model. The black lines are the wells positions. The Well 1 is the one in the left, the Well 2 goes in the middle, and the one to the right is the Well 3.

For the starting model on figure 3, we use a smoothed version of the true model of figure 2.

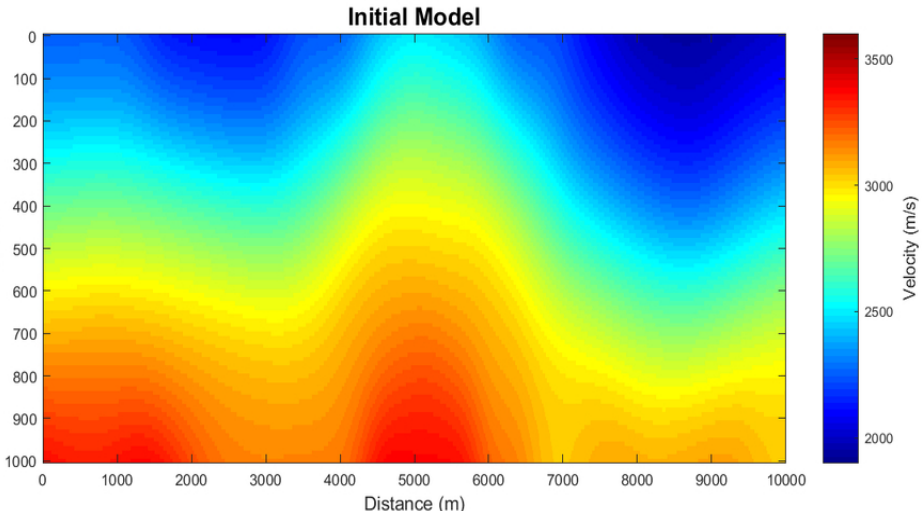

FIG. 3. The initial model is a smoothed version of the true velocity model.

Figure 4 shows the final model using a zero-offset PSPI migration to obtain the gradient. Most of the main features of the true model are recovered. We can observe some border effects, mainly due to the lack of information of the stack section at low fold. The shallow part of the model looks blurred and some events look discontinuous.

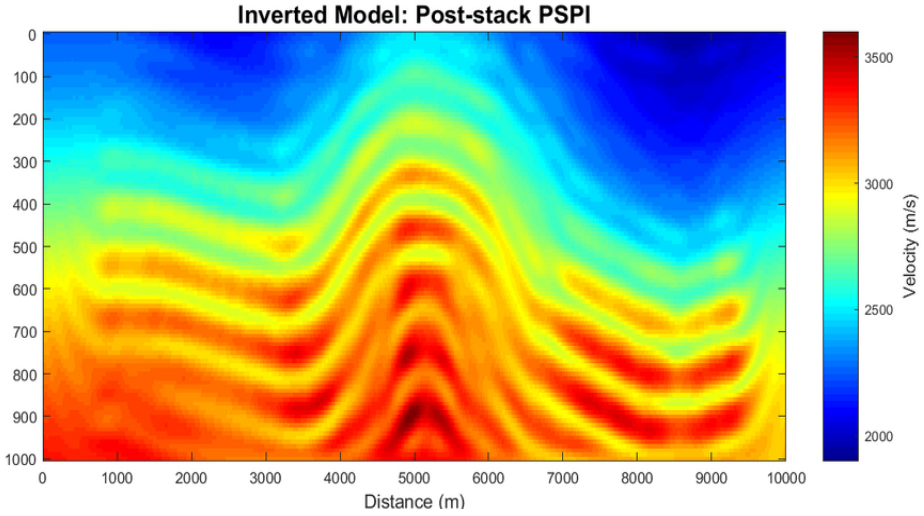

FIG. 4. Inverted model for the post-stack method using a zero-offset PSPI migration.

Now we changed the zero-offset PSPI migration to a explosive reflector based RTM and inverted model is shown on figure 5. The first thing that called our attention is the high velocity layers that were included in the right side of the model. Apparently, some unbalance amplitude came out from the RTM process in the area with lower coverage. However, the rest of the model looks to have more details then the PSPI one, inverting better the structures in the shallow area, and even making more clear a deep layer in the left side of the model.

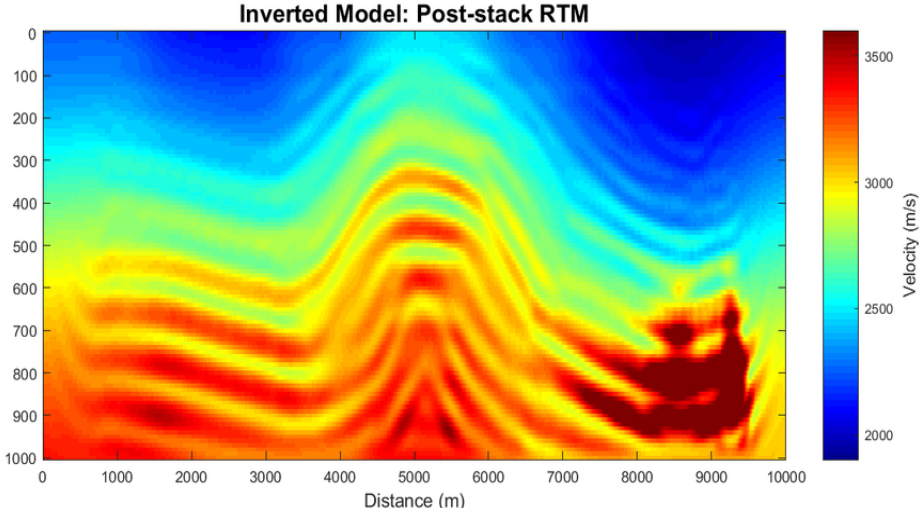

FIG. 5. Inverted model for the post-stack method using a explosive reflector based RTM.

The inversion, for both migrations processes, are driven by the sonic logs. In others words, the model is minimized at the sonic logs locations and extrapolated for the rest of

the model. Figure 6 shows the deviation at the well location for a) using the PSPI migration, and b) with the RTM. For the Well 2 (blue line) the deviation shows similar behavior for both methods, but Wells 1 (black line) and 3 (red line) are better inverted for the PSPI migration.

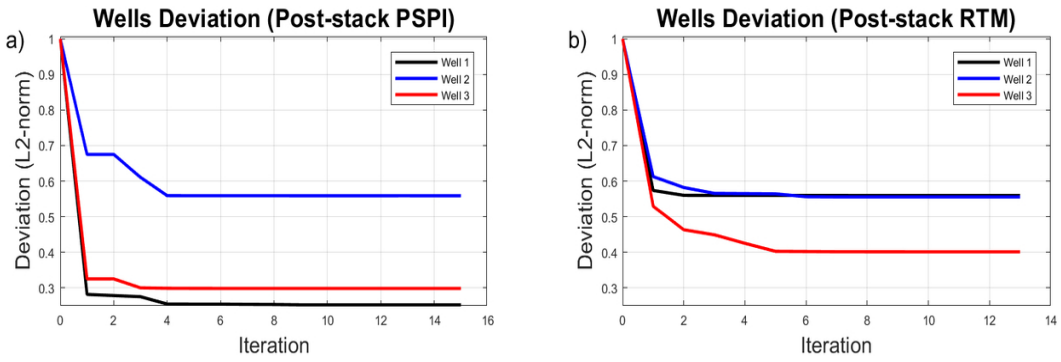

FIG. 6. Deviations of the Wells 1 (black line), 2 (blue line), and 3 (red line), for the a) PSPI and b) RTM methods. The PSPI shows to me more effective in the well optimization.

Checking the model deviation per iteration of figure 7, the inversion using the PSPI migration (red line) did a better job then the RTM one (blue line). By looking back to the inverted model of figures 4 and 5, the RTM model looks to have higher resolution, but the PSPI inversion leaded to velocities closer to the true model.

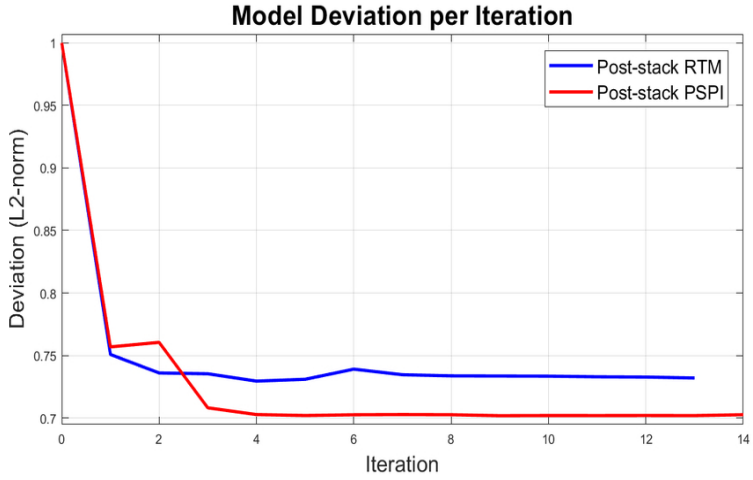

FIG. 7. Model deviation of the RTM (blue line) and PSPI (red line) methods. The PSPI one shows to lead to a model closer to the true velocity.

In the end, for the post-stack method, the PSPI migration shows to have done a better job than the RTM, resulting in a velocity model that is overall closer to the true model.

FastWI RTM vs PSPI: Marmousi Model

The FastWI showed to be effective on a simple model, with fairly similar inversions using the RTM and PSPI migrations to obtain the gradient. Now we are going to present the difference of the inversions in the Marmousi model of figure 8. On the same figure, it is drawn the single sonic log (black line) used to calibrate the gradient.

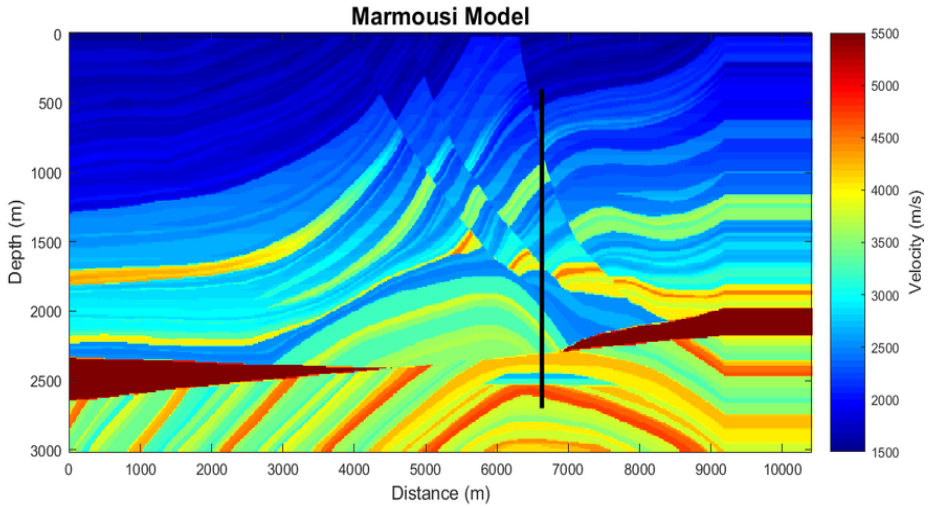

FIG. 8. Marmousi model. The sonic log is represented by the vertical black line close to the center of the model.

The stacked section used as the input data is shown on figure 9. It was obtained by stacking the NMO corrected CDPs using a velocity analysis output. It is possible to observe a collection of diffractions in central portion of the stack section, due the strong faults of the model (figure 8). The high velocity bodies in the deeper area of the model cause internal multiples observed clearly in the left side of the stacked section at 2.5 seconds. In opposite to the stacked section of the simple model, for the Marmousi we were able to completely remove the direct arrivals without attacking the primaries, by simply doing a forward modeling using the water velocity (resulting in shots with only the direct arrival), and subtracting it from the shots before stacking.

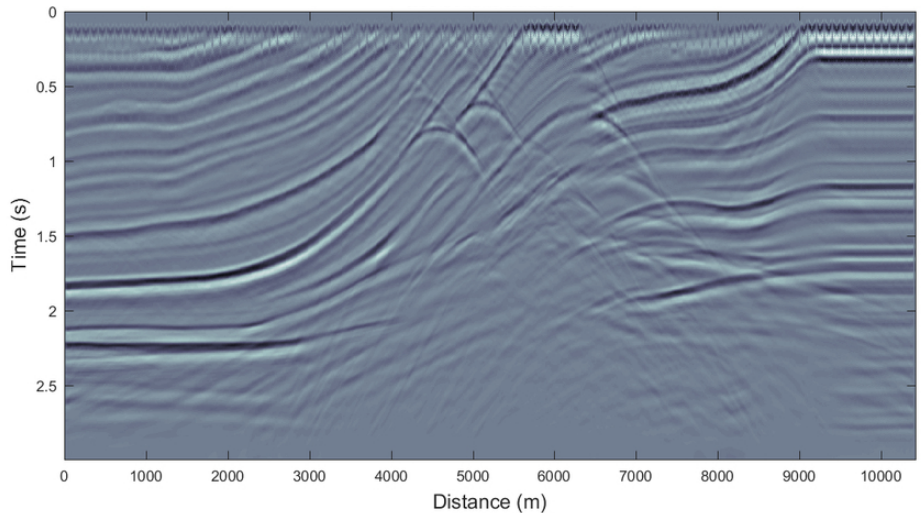

FIG. 9. The Marmousi stacked section used as input in the post-stack method.

Figure 10 shows the initial model used for the tests. It was obtained by convolving the true model of figure 8 with a 2D Gaussian window.

For this test, we are using a single sonic log (figure 8). We use the multiscale method

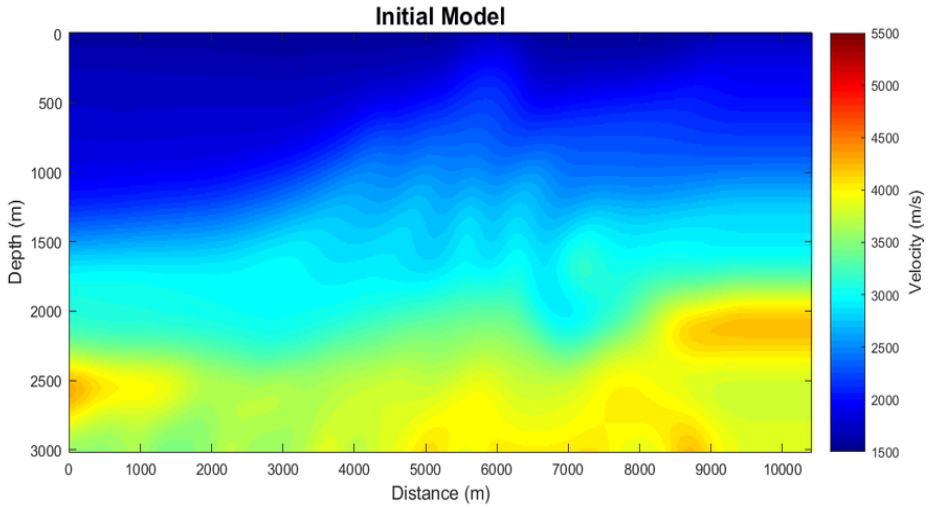

FIG. 10. Marmousi model. The sonic log is represented by the vertical black line close to the center of the model

by inverting first the lower frequencies and increase the frequency on later iterations. First, we applied the FastWI using a zero-offset PSPI migration and the inverted model is shown on figure 11. The main characteristics of the true model (figure 8) were recovered, and we can even note the large faults in the center of the model. However, the deeper area of the models was not correctly inverted, which is more evident in the high velocity body on both sides of the model.

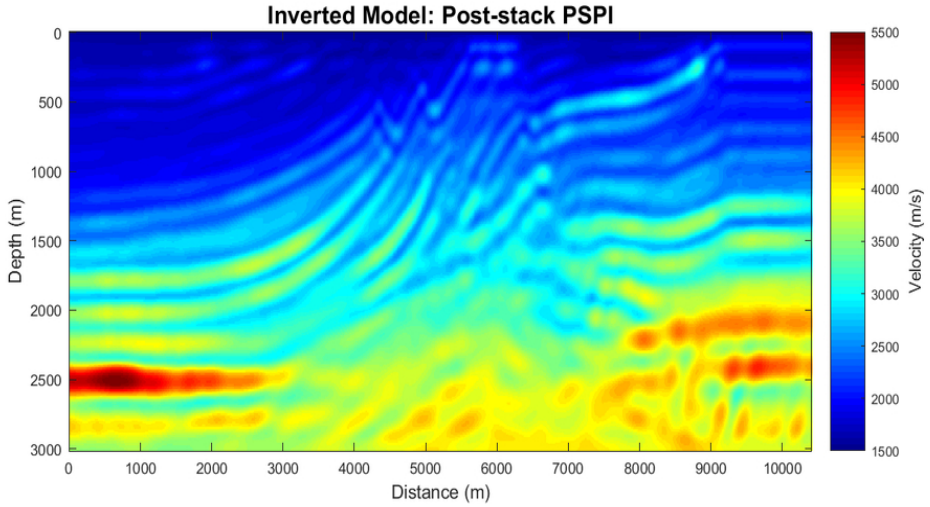

FIG. 11. Inverted model using a zero-offset PSPI migration. The main features of the true model of figure 8 were recovered, but the deeper areas are not so clear when compared to the inversion with the RTM (figure 12).

Replacing the zero-offset PSPI migration by a explosive reflector based RTM, we got the inversion shown on figure 12. The first thing we notice when we compared it to the PSPI inversion of figure 11 is the the RTM inversion did a better job in the deep portion of the model, and it is even more evident on the high velocity bodies, that look more continuous and with a closer velocity to the true model. On the shallower area, the inversions with

the RTM and PSPI migrations look to be close to each other, with the inversion with RTM showing a slightly higher resolution and with velocities of some areas looking more similar to the true model of figure 8. However, in the shallow area, it is difficult to evaluate which one of the really worked better by just comparing the images.

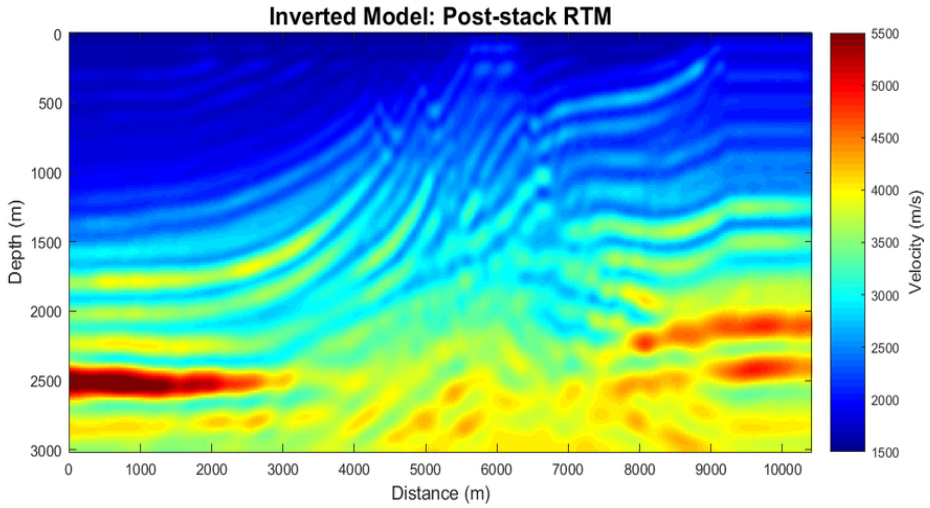

FIG. 12. Inverted model using a explosive reflector based RTM. It shows a higher resolution than the model inverted using the zero-offset PSPI migration (figure 11).

Now, by analyzing the deviation of each updated model to the sonic log (figure 13), the inversion with the PSPI migration has a slightly lower error than the inversion with th RTM, but the difference is close to 1% of the normalized deviation. So,at the well location, we can say that both inversions are pretty close.

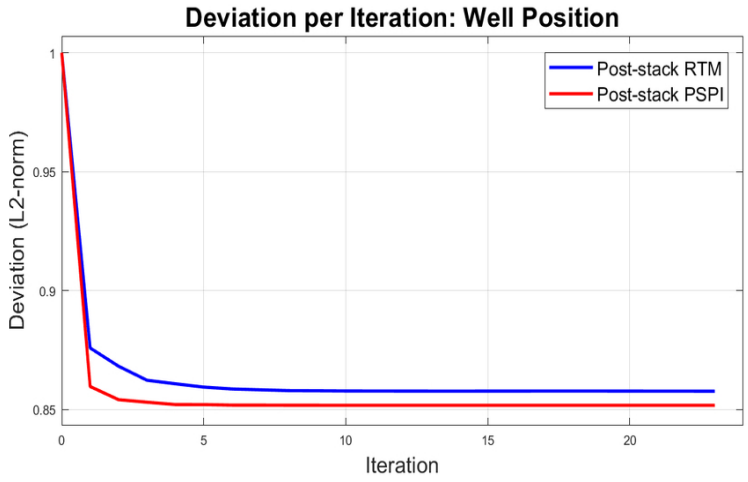

FIG. 13. Sonic log deviation of the RTM (blue line) and PSPI (red line) methods. At the well position, the inversion with the PSPI migration has is slightly closer to the true model.

In the other hand, when we analyze the model deviation per iteration (figure 14), we see, for the final model, a slightly advantage for the inversion using the RTM. However, we noticed that the model with the lowest error is the one in the first iteration. For the subsequent iterations, the inverted model starts to diverge to the true model, ending close to the final inversion using the PSPI migration. But by looking back at the final models

using the RTM (figure 12) and PSPI (figure 11) migrations, the first one worked better in the deeper area. Is this suggesting that the inversion with the PSPI migration is doing a better job in the shallower portion of the model (where the geology is simpler) than the inversion with the RTM? Well, if we look back to the results of the last section, when we compared both inversions on a simpler model, the inversions using the PSPI migration showed to be more stable and to result in an overall better model. So, this "compensation" in the model deviation of figure 14 can be the result of a less stable model inverted by using the RTM in the shallower part. But, in a more complex model, The inversion using the RTM resulted in an overall better model.

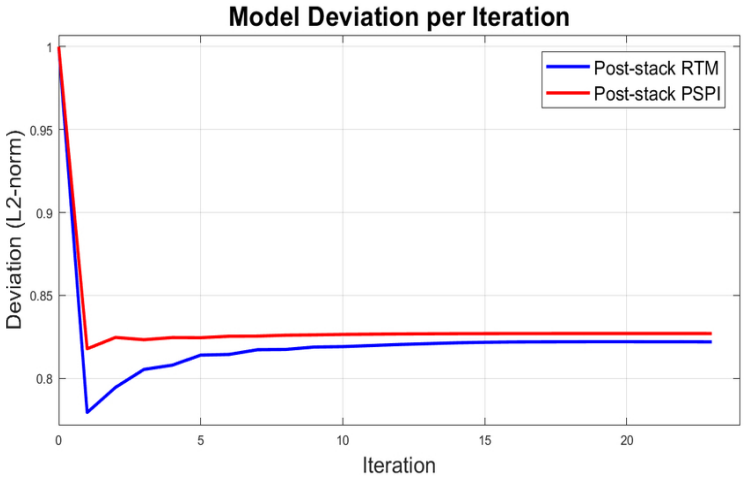

FIG. 14. Model deviation of the RTM (blue line) and PSPI (red line) methods. The RTM looks to work better for lower frequencies, but as we start to go to higher frequencies, the model starts to diverge.

CONCLUSIONS

In this work we compared the use of two different depth migrations to obtain the gradient: the zero-offset PSPI and the explosive reflector based RTM. For the simpler model, the RTM shows to invert a model with higher resolution, but with more artifacts and over-corrected velocities, but the PSPI leaded to an inverted model that, in overall, is closer to the true model. However, the opposite happens when we do the comparison in the Marmousi model. As the geology gets more complex, the inversion using the RTM does a better job, mostly in the deeper area of the model. In the end of the day, which depth migration to select for the FastWI depends on the computational resources of the processor (with the advantage for the PSPI) and the complexity of the geology in the studying area (as it gets more complex, the advantage goes to the RTM). For our simulation, the PSPI migration shows to be, in the overall scenario (the gain in costs for the RTM does not represent a linear gain in quality), the best option.

ACKNOWLEDGMENTS

The authors thank the sponsors of CREWES for continued support. This work was funded by CREWES industrial sponsors and NSERC (Natural Science and Engineering Research Council of Canada) through the grant CRDPJ 461179-13.

REFERENCES

Bishop, T. N., and Spongberg, M. E., 1984, Seismic tomography: A case study: SEG Technical Program Expanded Abstracts, **313**, 712–713.

Chipman, J. S., 1999, Linear restrictions, rank reduction, and biased estimation in linear regression: Linear Algebra and its Applications, **289**, No. 1, 55 – 74.

Cutler, R. T., Bishop, T. N., Wyld, H. W., Shuey, R. T., Kroeger, R. A., Jones, R. C., and Rathbun, M. L., 1984, Seismic tomography: Formulation and methodology: SEG Technical Program Expanded Abstracts, **312**, 711–712.

Fatti, J. L., Smith, G. C., Vail, P. J., Strauss, P. J., and Levitt, P. R., 1994, Detection of gas in sandstone reservoirs using avo analysis: A 3-d seismic case history using the geostack technique: Geophysics, **59**, No. 9, 1362–1376.

Gazdag, J., and Sguazzero, P., 1984, Migration of seismic data by phase shift plus interpolation: Geophysics, **49**, No. 2, 124–131.

Guarido, M., Lines, L., and Ferguson, R., 2014, Full waveform inversion - a synthetic test using the pspi migration: CREWES Research Report, **26**, 26.1–26.23.

Guarido, M., Lines, L., and Ferguson, R., 2015, Full waveform inversion: a synthetic test using pspi migration: SEG Technical Program Expanded Abstract, **279**, 1456–1460.

Guarido, M., Lines, L., and Ferguson, R., 2016, Fwi without tears: a forward modeling free gradient: CREWES Research Report, **28**, 26.1–26.20.

Guarido, M., Lines, L., and Ferguson, R., 2017a, Forward modeling-free full waveform inversion with well calibration: CREWES Research Report, **29**.

Guarido, M., Lines, L., and Ferguson, R., 2017b, Fwi without tears: a forward modeling-free gradient: SEG Technical Program Expanded Abstract, 1588–1593.

Lailly, P., 1983, The seismic inverse problem as a sequence of before stack migrations: Conference on inverse scattering, theory and application: Society of Industrial and Applied Mathematics, Expanded Abstracts, 206–220.

Langan, R. T., Lerche, I., Cutler, R. T., Bishop, T. N., and Spera, N. J., 1984, Seismic tomography: The accurate and efficient tracing of rays through heterogeneous media: SEG Technical Program Expanded Abstracts, **314**, 713–715.

Lindseth, R. O., 1979, Synthetic sonic logs-a process for stratigraphic interpretation: Geophysics, **44**, No. 1, 3–26.

Margrave, G., Ferguson, R., and Hogan, C., 2010, Full waveform inversion with wave equation migration and well control: CREWES Research Report, **22**, 63.1–63.20.

Margrave, G., Yedlin, M., and Innanen, K., 2011, Full waveform inversion and the inverse hessian: CREWES Research Report, **23**, 77.1–77.13.

Pica, A., Diet, J. P., and Tarantola, A., 1990, Nonlinear inversion of seismic reflection data in a laterally invariant medium: Geophysics, **55**, No. 2, R59–R80.

Pratt, R. G., Shin, C., and Hick, G. J., 1998, Gauss-newton and full newton methods in frequency-space seismic waveform inversion: Geophysical Journal International, **133**, No. 2, 341–362.

Romahn, S., and Innanen, K., 2016, Immi: the role of well calibration in the context of high geological complexity: CREWES Research Report, **28**, 66.1–66.17.

Shuey, R. T., 1985, A simplification of the zoeppritz equations: Geophysics, **50**, No. 4, 609–614.

Tarantola, A., 1984, Inversion of seismic reflection data in the acoustic approximation: Geophysics, **49**, No. 8, 1259–1266.

Virieux, J., and Operto, S., 2009, An overview of full-waveform inversion in exploration geophysics: Geophysics, **74**, No. 6, WCC1–WCC26.

Warner, M., and Guasch, L., 2014, Adaptive waveform inversion: Theory: SEG Technical Program Expanded Abstracts, **207**, 1089–1093.

Wenyong, P., Margrave, G., and Innanen, K., 2013, On the role of the deconvolution imaging condition in full waveform inversion: CREWES Research Report, **25**, 72.1–72.19.